

# Influence of quantum interference on the polarization and angular distribution of x-ray radiation following electron-impact excitation of highly charged H-like and He-like ions

Z. B. Chen, C. Z. Dong,\* L. Y. Xie, and J. Jiang

Key Laboratory of Atomic and Molecular Physics & Functional Materials of Gansu Province, College of Physics and Electronic Engineering, Northwest Normal University, Lanzhou 730070, China  
and Joint Laboratory of Atomic and Molecular Physics, Northwest Normal University and Institute of Modern Physics of Chinese Academy of Sciences, Lanzhou 730070, China

(Received 10 April 2014; published 7 July 2014)

Detailed calculations are carried out for the polarization properties and angular distribution of the x-ray photoemission of highly charged H-like and He-like ions following electron-impact excitation using a fully relativistic distorted-wave method. The contributions of the magnetic quadrupole ( $M2$ ) to the subsequent characteristic x-ray emission are investigated systematically. For the Lyman- $\alpha_1$  ( $2p_{3/2} \rightarrow 1s_{1/2}$ ) radiation of H-like ions, it is shown that the interference between the leading electric dipole ( $E1$ ) decay and the much weaker  $M2$  decay may significantly reduce the polarization and slightly increase the angular distribution of the emitted x-rays, these characteristics are very similar to the conclusions regarding the radiative electron capture process [G. Weber *et al.*, *Phys. Rev. Lett.* **105**, 243002 (2010)]. However, for the  $2s_{1/2}2p_{3/2}(J=1) \rightarrow 1s_{1/2}2s_{1/2}(J=1)$  radiation of He-like ions, the  $E1$ - $M2$  interference leads to an obvious increase in polarization and a large decrease in the angular distribution of the x-ray photoemission, which is contrary to the Lyman- $\alpha_1$  line of H-like ions. And all these characters strongly depend on the atomic number and the incident electron energy.

DOI: 10.1103/PhysRevA.90.012703

PACS number(s): 34.80.Dp, 34.80.Lx

## I. INTRODUCTION

The polarization of x-ray line emission from highly charged ions undergoing collisions with an electron beam has been a topic of continuous fundamental interest for decades. The understanding of the processes is important not only to diagnose electron distribution anisotropy in high-temperature plasmas, but also to provide information on both incident electrons and excitation dynamics. Recently, an important diagnostic tool has been successfully developed and applied to describe both the angular and the energy distributions of nonthermal electrons existing in astrophysical and laboratory plasmas, particularly in solar corona plasmas [1–3], tokamak plasmas [4], and laser-produced plasmas [5–9].

During the last few years, the degree of linear polarization of x-ray emission from highly charged ions colliding with an electron beam has been extensively investigated. With respect to experiments, several important polarization measurements were reported for H-like and He-like few-electron ions [10–20]. With respect to theory, Reed *et al.* [21] have investigated the relativistic effects on the degree of linear polarization of x-ray emission following electron-impact excitation (EIE) for highly charged H-like and He-like ions. Fontes *et al.* [22] have studied the contribution of the Breit interaction to the collision strength and the degree of linear polarization of the radiation emission following EIE of He-like ions. Sharma *et al.* [23] have studied the degree of linear polarization of the  $ns_{1/2}$ - $np_{1/2}$  and  $ns_{1/2}$ - $np_{3/2}$  resonance transitions for singly charged  $\text{Mg}^+$  ( $n=3$ ),  $\text{Ca}^+$  ( $n=4$ ),  $\text{Zn}^+$  ( $n=4$ ),  $\text{Cd}^+$  ( $n=5$ ), and  $\text{Ba}^+$  ( $n=6$ ) ions with the use of a fully relativistic distorted-wave (RDW) method. Amaro *et al.* [24] have analyzed the angular correlation and the degree of linear polarization for radiation emitted in two-photon decay of H-like ions. There are also many other theoretical

studies on the degree of linear polarization [25–39]. However, most of these works have paid attention to the decay from individual magnetic sublevels to the ground state; there is a lack of studies on various transitions among the different excited states. In addition, to our knowledge, most previous theoretical investigations have taken into account only a single type of radiation transition, such as  $E1$  or  $M2$ . In fact, x-ray lines emitted by highly charged ions arise not only from the optically allowed  $E1$  transitions but also from the forbidden electric and magnetic transitions. Sometimes, two successive multipole orders of the same parity, one electric and the other magnetic, are simultaneously allowed by the angular momentum selection rules. This concerns, in most cases, mixtures of dipoles and quadrupoles [40]. For example, for H-like ions, strong interference effects between  $E1$  and  $M2$  transitions have been found for the Lyman- $\alpha_1$  ( $2p_{3/2} \rightarrow 1s_{1/2}$ ) decay of uranium, following radiative electron capture (REC) into the  $2p_{3/2}$  level of initially bare ions [41]. And these effects, especially the  $M2$  contributions, can significantly modify the angular distribution of the linear polarization for Lyman- $\alpha_1$  ( $2p_{3/2} \rightarrow 1s_{1/2}$ ) radiation. This predicted phenomenon has recently been observed and confirmed experimentally [42]. For He-like ions, the most recent computations show that the polarization of the  $K\alpha_1$  ( $1s2p_{3/2}^3P_2 \rightarrow 1s^2^1S_0$ ) line following REC can also be significantly affected by multipole mixing between the leading  $M2$  and hyperfine-induced  $E1$  components of  $1s2p^3P_2, F_i \rightarrow 1s^2^1S_0, F_f$  transitions [43], and this  $E1$ - $M2$  mixing strongly depends on the nuclear properties of the considered isotopes. Therefore, some similar effects should also be expected for these characteristic emissions from other few-electron ions and other dynamical processes.

In the present work, we apply the multiconfiguration Dirac-Fock method (MCDF) and fully RDW method to explore an interference between the  $E1$  and the  $M2$  transition for the Lyman- $\alpha_1$  ( $2p_{3/2} \rightarrow 1s_{1/2}$ ) line of H-like  $\text{Mo}^{41+}$ ,  $\text{Au}^{78+}$ , and  $\text{U}^{91+}$  ions and the  $2s_{1/2}2p_{3/2}(J=1) \rightarrow 1s_{1/2}2s_{1/2}(J=1)$

\*dongcz@nwnu.edu.cn

line of He-like  $\text{Mo}^{40+}$ ,  $\text{Au}^{77+}$ , and  $\text{U}^{90+}$  ions following EIE processes. The influences of  $E1$  and  $M2$  interference on the polarization and angular properties of subsequent radiation are discussed in detail. The paper is organized as follows. In Sec. II we describe the theoretical approach and computational details. In Sec. III we present our results for the effects of interference on the polarization and angular distribution of x-ray radiation following EIE of highly charged H-like and He-like ions. Finally, we end with some conclusions in Sec. IV.

## II. THEORETICAL METHODS

In the present work, the target-state wave functions are generated with the use of the atomic structure package

GRASP92 [44] based on the MCDF method. The cross sections for EIE of individual magnetic sublevels of H-like and He-like ions are calculated using a newly developed fully RDW program, REIE06 [37,45], in which the continuum electron wave functions are produced by the component COWF of the RATIP package [46] by solving the coupled Dirac equation in which the exchange effect between the bound and the continuum electrons are considered.

It is convenient to choose the  $z$  axis to be the direction of the motion of the incident electron, and then the  $z$  component of the incident electron orbital angular momentum is 0, namely,  $m_{li} = 0$ . In this case, the EIE cross section of the target ion from the initial state  $\beta_i J_i M_i$  to the final state  $\beta_f J_f M_f$  is given by [47,48]

$$\begin{aligned} \sigma_{\varepsilon_i}(\beta_i J_i M_i - \beta_f J_f M_f) = & \frac{2\pi a_0^2}{k_i^2} \sum_{l_i, l'_i, j_i, j'_i, m_{s_i}, l_f, j_f, m_f} \sum_{J, J', M} (i)^{l_i - l'_i} [(2l_i + 1)(2l'_i + 1)]^{1/2} \exp[i(\delta_{\kappa_i} - \delta_{\kappa'_i})] C\left(l_i \frac{1}{2} m_{li} m_{si}; j_i m_i\right) \\ & \times C\left(l'_i \frac{1}{2} m_{l'_i} m_{s'_i}; j'_i m_i\right) C(J_i j_i M_i m_i; J M) C(J_i j'_i M_i m_i; J' M) C(J_f j_f M_f m_f; J M) \\ & \times C(J_f j'_f M_f m_f; J' M) R(\gamma_i, \gamma_f) R(\gamma'_i, \gamma'_f). \end{aligned} \quad (1)$$

Here, the subscripts  $i$  and  $f$  denote the initial and final states. The  $\varepsilon_i$  is the incident electron energy (in Rydberg).  $a_0$  is the first Bohr radius. The  $C$ 's and  $R$ 's are Clebsch-Gordan coefficients and collision matrix elements, respectively.  $\gamma_i = \varepsilon_i l_i j_i \beta_i J_i J M$  and  $\gamma_f = \varepsilon_f l_f j_f \beta_f J_f J M$ , where  $J$  and  $M$  are the quantum numbers corresponding to the total angular momentum of the collisional system (target ion plus free electron) and its  $z$  component, respectively;  $\beta_i$  represents all additional quantum numbers required to specify the initial states of the target ion in addition to its total angular momentum  $J_i$  and  $z$  component  $M_i$ , respectively. The quantity  $\beta_f$  has a similar meaning for the final state.  $m_{s_i}$ ,  $l_i$ ,  $j_i$ ,  $m_{l_i}$ , and  $m_i$  are the quantum numbers for the spin, the orbital angular momentum, the total angular momentum, and its  $z$  component, respectively, for the incident electron  $e_i$ ;  $\delta_{\kappa_i}$  is the phase factor for the continuum electron.  $\kappa$  is the relativistic quantum number, which is related to the orbital and total angular momentum  $l$  and  $j$ .  $k_i$  is the relativistic wave number of the incident electron and is given by

$$k_i^2 = \varepsilon_i \left(1 + \frac{\alpha^2 \varepsilon_i}{4}\right), \quad (2)$$

where  $\alpha$  is the fine-structure constant. It turns out that  $R(\gamma_i, \gamma_f)$  is independent of  $M$  and can be written as

$$R(\gamma_i, \gamma_f) = \langle \Psi_{\gamma_f} | \sum_{p, q, p < q}^{N+1} (V_{\text{Coul}} + V_{\text{Breit}}) | \Psi_{\gamma_i} \rangle, \quad (3)$$

where  $\Psi_{\gamma_i}$  and  $\Psi_{\gamma_f}$  are the antisymmetric  $N + 1$  electron wave functions for the initial and final states of the impact systems, respectively.  $V_{\text{Coul}}$  is the Coulomb operator, and  $V_{\text{Breit}}$  is the Breit operator [44].

In order to consider the  $E1$ - $M2$  interference effect, a theory of the polarization of radiation emitted from an aligned ion in any one-photon transition involving two different electromag-

netic multipoles was developed by Bensaid *et al.* [40]. For radiation lines from  $J = 3/2$  to  $J = 1/2$  and from  $J = 1$  to  $J = 1$ , the linear polarization at the observation angle can be represented as [40]

$$\eta(\theta) = \frac{P \sin^2 \theta}{1 - g(E1, M2) P \cos^2 \theta}, \quad (4)$$

where  $P$  is the degree of polarization at the observation angle of  $90^\circ$ ,

$$P = \frac{A}{B + C}. \quad (5)$$

For the  $J = 3/2$  to  $J = 1/2$  lines,

$$A = (\sigma_{1/2} - \sigma_{3/2})(3A_{E1} - 3A_{M2} + 2\sqrt{3A_{E1}A_{M2}}), \quad (6)$$

$$B = (5\sigma_{1/2} + 3\sigma_{3/2})A_{E1} + (3\sigma_{1/2} + 5\sigma_{3/2})A_{M2}, \quad (7)$$

$$C = 2(\sigma_{1/2} - \sigma_{3/2})\sqrt{3A_{E1}A_{M2}}, \quad (8)$$

and

$$g(E1, M2) = \frac{A_{E1} - A_{M2} + 2\sqrt{3}\sqrt{A_{E1}A_{M2}}}{A_{E1} - A_{M2} - 2\frac{\sqrt{3}}{3}\sqrt{A_{E1}A_{M2}}}. \quad (9)$$

The angular distribution of radiation can be written as

$$\begin{aligned} W(\theta) = \langle W \rangle \left\{ 1 + \left[ \frac{A_{E1} - A_{M2} + 2\sqrt{3}\sqrt{A_{E1}A_{M2}}}{A_{E1} + A_{M2}} \right. \right. \\ \left. \left. \times \frac{1}{2} \frac{\sigma_{3/2} - \sigma_{1/2}}{\sigma_{3/2} + \sigma_{1/2}} P_2(\cos \theta) \right] \right\}, \end{aligned} \quad (10)$$

where  $A_{E1}$  and  $A_{M2}$  are the pure  $E1$  transition and pure  $M2$  transition probability, respectively.  $\langle W \rangle$  is the mean intensity [40], and  $P_2(\cos \theta)$  is the second-order Legendre polynomial.  $\sigma_{1/2}$  and  $\sigma_{3/2}$  are the EIE cross sections from

the initial state to the final magnetic sublevels  $M_f = 1/2$  and  $M_f = 3/2$ , respectively.

For the  $J = 1$  to  $J = 1$  lines,

$$A = (\sigma_1 - \sigma_0)(A_{E1} + A_{M2} + 2\sqrt{A_{E1}A_{M2}}), \quad (11)$$

$$B = (\sigma_0 + 3\sigma_1)(A_{E1} + A_{M2}), \quad (12)$$

$$C = 2(\sigma_0 - \sigma_1)\sqrt{A_{E1}A_{M2}} \quad (13)$$

and

$$g(E1, M2) = \frac{A_{E1} + A_{M2} - 6\sqrt{A_{E1}A_{M2}}}{A_{E1} + A_{M2} + 2\sqrt{A_{E1}A_{M2}}}. \quad (14)$$

The angular distribution of radiation can be written as

$$W(\theta) = \langle W \rangle \left\{ 1 + \left[ \frac{A_{E1} + A_{M2} - 6\sqrt{A_{E1}A_{M2}}}{A_{E1} + A_{M2}} \times \frac{1}{2} \frac{\sigma_0 - \sigma_1}{\sigma_0 + 2\sigma_1} P_2(\cos \theta) \right] \right\}, \quad (15)$$

where  $\sigma_0$  and  $\sigma_1$  are the EIE cross sections from the initial state to magnetic sublevels  $M_f = 0$  and  $M_f = 1$  of the final state, respectively.

### III. RESULTS AND DISCUSSION

#### A. Comparisons of transition probability and linear polarization

In Table I, the calculated transition probabilities of the Lyman- $\alpha_1$  ( $2p_{3/2} \rightarrow 1s_{1/2}$ ) transition line of H-like  $\text{Mo}^{41+}$ ,  $\text{Au}^{78+}$ , and  $\text{U}^{91+}$  ions and the  $2s_{1/2}2p_{3/2}(J=1) \rightarrow$

TABLE I. Comparison of the transition probabilities ( $\text{s}^{-1}$ ) of the Lyman- $\alpha_1$  line ( $2p_{3/2} \rightarrow 1s_{1/2}$ ) for H-like ions and the  $2s_{1/2}2p_{3/2}(J=1) \rightarrow 1s_{1/2}2s_{1/2}(J=1)$  transition line for He-like ions between the present calculated results and the existing theoretical results. Superscript B, Babushkin gauge; superscript C, Coulomb gauge.  $R[n]$  means  $R \times 10^n$ .

Ion	Type	Present	Others
H-like			
$\text{Mo}^{41+}$	$E1$	1.91[15] <sup>C</sup> , 1.91[15] <sup>B</sup>	1.90[15] <sup>a</sup>
	$M2$	4.67[11]	
$\text{Au}^{78+}$	$E1$	2.07[16] <sup>C</sup> , 2.23[16] <sup>B</sup>	2.23[16], <sup>a</sup> 2.02[16] <sup>c</sup>
	$M2$	7.91[13]	
$\text{U}^{91+}$	$E1$	3.69[16] <sup>C</sup> , 3.93[16] <sup>B</sup>	3.95[16], <sup>a</sup> 3.92[16], <sup>b</sup> 3.34[16] <sup>d</sup>
	$M2$	2.80[14]	2.82[14] <sup>b</sup>
He-like			
$\text{Mo}^{40+}$	$E1$	3.29[14] <sup>C</sup> , 3.29[14] <sup>B</sup>	
	$M2$	4.47[11]	
$\text{Au}^{77+}$	$E1$	6.52[15] <sup>C</sup> , 6.72[15] <sup>B</sup>	6.22[15] <sup>c</sup>
	$M2$	7.84[13]	
$\text{U}^{90+}$	$E1$	1.02[16] <sup>C</sup> , 1.22[16] <sup>B</sup>	1.10[16] <sup>d</sup>
	$M2$	2.77[14]	

<sup>a</sup>From Ref. [49].

<sup>b</sup>From Ref. [41].

<sup>c</sup>From Ref. [52].

<sup>d</sup>From Ref. [51].

$1s_{1/2}2s_{1/2}(J=1)$  transition line of He-like  $\text{Mo}^{40+}$ ,  $\text{Au}^{77+}$ , and  $\text{U}^{90+}$  ions are listed along with the existing theoretical values. It is found that the agreement with the different calculations is good in general for both the  $E1$  and the  $M2$  transition probabilities. For example, for the Lyman- $\alpha_1$  radiative line of  $\text{U}^{91+}$  ions, the present  $E1$  and  $M2$  transition probabilities are  $3.93 \times 10^{16}$  and  $2.80 \times 10^{14} \text{ s}^{-1}$ , respectively. These results are in good agreement with the  $E1$  results  $3.95 \times 10^{16} \text{ s}^{-1}$  by the calculations of Pal'chikov [49] and  $3.34 \times 10^{16} \text{ s}^{-1}$  in the NORAD Atomic Data [50] by the calculations of Nahar *et al.* [51] and the  $E1$  result  $3.92 \times 10^{16} \text{ s}^{-1}$  and  $M2$  result  $2.82 \times 10^{14} \text{ s}^{-1}$  given by Surzhykov *et al.* [41]. For the  $2s_{1/2}2p_{3/2}(J=1) \rightarrow 1s_{1/2}2s_{1/2}(J=1)$  transition line of He-like  $\text{Au}^{77+}$  and  $\text{U}^{90+}$  ions, the present  $E1$  transition probabilities,  $6.72 \times 10^{15}$  and  $1.22 \times 10^{16} \text{ s}^{-1}$ , also agree very well with the results  $6.22 \times 10^{15}$  and  $1.10 \times 10^{16} \text{ s}^{-1}$  in the NORAD Atomic Data calculated by Nahar *et al.* [51,52], respectively. In addition, the present calculated transition probabilities in both the Babushkin and the Coulomb gauges are reasonably consistent with each other.

For the sake of further explaining the reliability of the present calculations, in Table II, the calculated linear polarizations of the Lyman- $\alpha_1$  ( $2p_{3/2} \rightarrow 1s_{1/2}$ ) line without consider interference effects for highly charged H-like ions are listed, along with the existing theoretical and experimental values. It is shown that all the theoretical values are quite close to each other. The present results are in very good agreement with the previous relativistic convergent close-coupling calculations of Bostocket *et al.* [53] and experimental values within the experimental error. Taking  $\text{Fe}^{25+}$  ions, for example, the present polarization is  $-0.111$  at incident energy 120 keV compared with the theoretical result  $-0.114$  and the experimental measurement  $-0.236 \pm 0.109$  performed on the Livermore EBIT [19]. An agreement of  $<3\%$  is quoted for the differences between the relativistic convergent close-coupling results and

TABLE II. Comparison of polarization of the Lyman- $\alpha_1$  line for highly charged H-like ions between the present calculated results and other experimental and theoretical ones. The two sets of experimental results for  $\text{Fe}^{25+}$  pertain to the two experiments outlined in Ref. [19].

Ion	Energy (keV)	Present	Theory	Experiment
$\text{Ar}^{17+}$	30	0.027	0.031 <sup>a</sup>	$-0.019 \pm 0.025^b$
	84	-0.135	-0.144 <sup>a</sup>	$-0.099 \pm 0.045^b$
$\text{Ti}^{21+}$	10.6	0.279	0.283 <sup>a</sup>	$0.214 \pm 0.066^c$
	24.7	0.122	0.127 <sup>a</sup>	$0.085 \pm 0.082^c$
$\text{Fe}^{25+}$	30	0.141	0.145 <sup>a</sup>	$0.071 \pm 0.034^b$ $0.051 \pm 0.111^b$
	120	-0.111	-0.114 <sup>a</sup>	$-0.236 \pm 0.109^b$ $-0.217 \pm 0.045^b$
$\text{Sn}^{49+}$	53.3	0.251		
	106.6	0.097		
$\text{Au}^{78+}$	287.1	0.024		
	358.8	-0.022		
$\text{U}^{91+}$	410.1	0.005		
	512.6	-0.041		

<sup>a</sup>Reference [53].

<sup>b</sup>Reference [19].

<sup>c</sup>Reference [17].

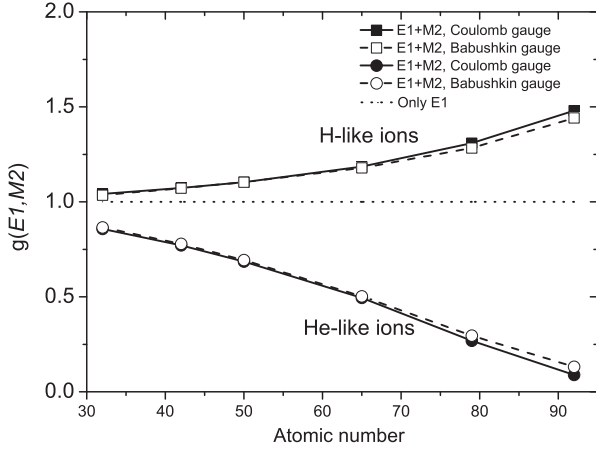


FIG. 1. The  $g(E1, M2)$  function for the Lyman- $\alpha_1$  ( $2p_{3/2} \rightarrow 1s_{1/2}$ ) transition line of H-like ions and the  $2s_{1/2}2p_{3/2}(J=1) \rightarrow 1s_{1/2}2s_{1/2}(J=1)$  transition line of He-like ions as a function of the nuclear charge  $z$ . Results from MCDHF calculations are shown in the Coulomb gauge (solid line) and Babushkin gauge (dashed line).

the present calculations. Therefore, the present calculations could be accurate enough for these highly charged ions.

### B. The $g(E1, M2)$ function

To understand how  $E1$ - $M2$  interference influences the polarization parameters, Fig. 1 displays the  $Z$ -dependence behavior of the  $g(E1, M2)$  function obtained from Eq. (9) and Eq. (14) for the  $2p_{3/2} \rightarrow 1s_{1/2}$  transition line of a H-like isoelectronic sequence and the  $2s_{1/2}2p_{3/2}(J=1) \rightarrow 1s_{1/2}2s_{1/2}(J=1)$  transition line of a He-like isoelectronic sequence, respectively. This function describes a typical coupling of the  $E1$  and the  $M2$  multipole components, which depends on the atomic structure of the ion and its coupling to the radiation field. If one did not consider the  $E1$ - $M2$  interference effects, the value of the  $g(E1, M2)$  function would equal a constant 1. As shown in Fig. 1, a strong variation of the  $g(E1, M2)$  function is found if the  $M2$  component is taken into account. However, for these two kinds of transitions, the behavior of the  $g(E1, M2)$  function is quite different. The  $g(E1, M2)$  function increases with increasing nuclear charge for the Lyman- $\alpha_1$  ( $2p_{3/2} \rightarrow 1s_{1/2}$ ) line of H-like ions, whereas it decreases for the  $2s_{1/2}2p_{3/2}(J=1) \rightarrow 1s_{1/2}2s_{1/2}(J=1)$  transition of He-like ions. It is also found that the  $g(E1, M2)$  function increases slowly as the atomic number increases for H-like ions, while it decreases rapidly for He-like ions. Figure 1 also shows the  $g(E1, M2)$  functions in the Babushkin gauge

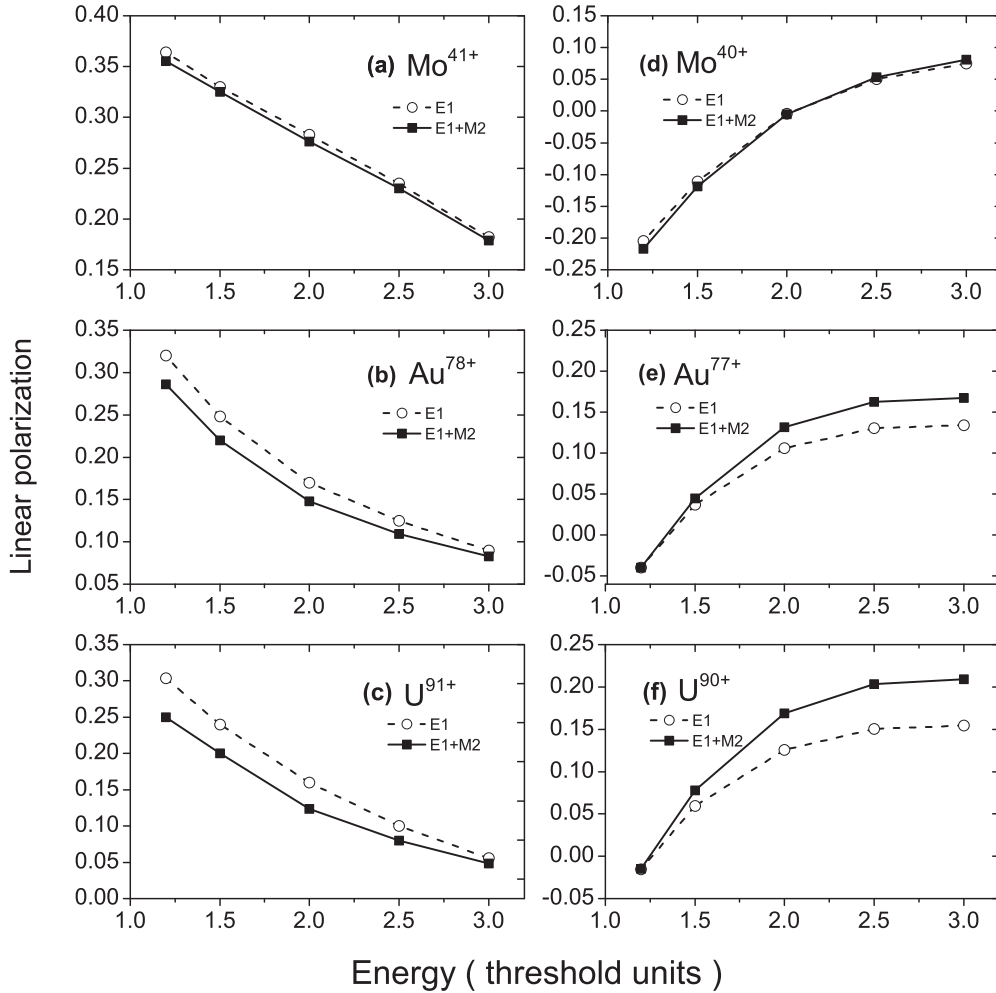


FIG. 2. The degree of linear polarization of the transition line  $2p_{3/2} \rightarrow 1s_{1/2}$  for H-like (left) and the transition line  $2s_{1/2}2p_{3/2}(J=1) \rightarrow 1s_{1/2}2s_{1/2}(J=1)$  for He-like (right) molybdenum, gold, and uranium ions as functions of the incident electron energy in threshold units.  $E1 + M2$  represents values with inclusion of  $E1$ - $M2$  interference, and  $E1$  represents inclusion of only the electric-dipole approximation.

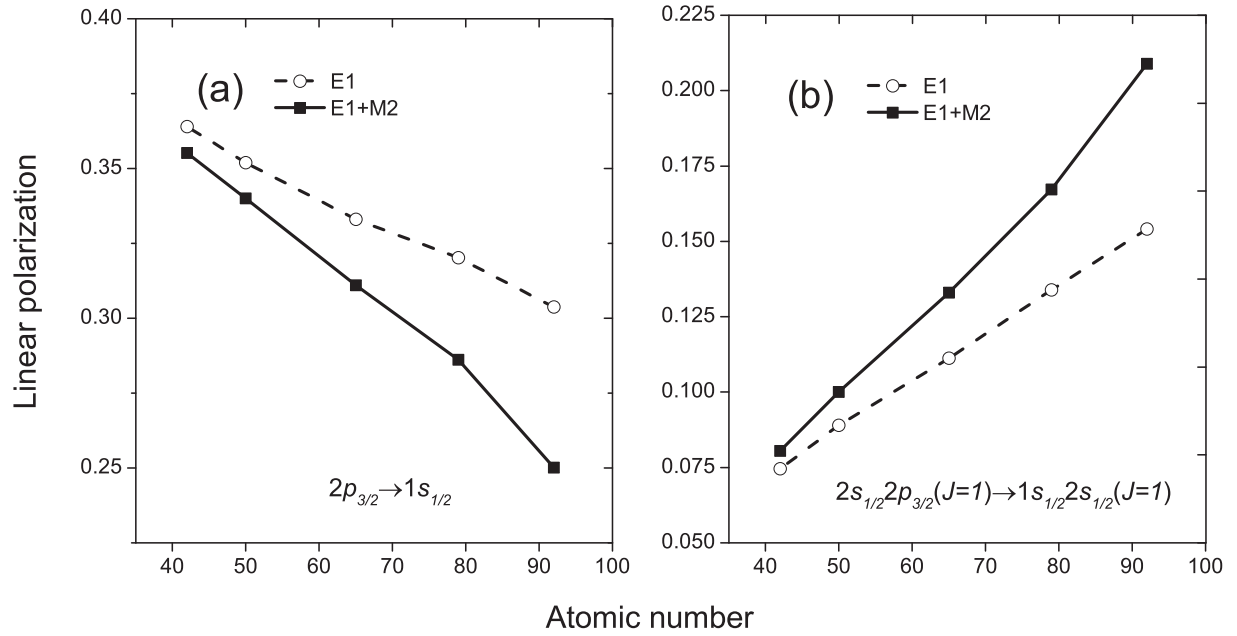


FIG. 3. The degree of linear polarization of the transition line  $2p_{3/2} \rightarrow 1s_{1/2}$  for H-like (left) ions and the transition line  $2s_{1/2}2p_{3/2}(J=1) \rightarrow 1s_{1/2}2s_{1/2}(J=1)$  for He-like (right) ions as functions of the atomic number at a given incident electron energy. E1 + M2 represents values with inclusion of  $E1$ - $M2$  interference, and E1 represents inclusion of only the electric-dipole approximation.

and Coulomb gauge. It is shown that the present calculated  $g(E1, M2)$  functions agree with each other very well, with a maximal discrepancy of  $<2\%$ . Therefore, the gauge differences can be neglected for the present investigations.

### C. The influence of interference on polarization properties

Figure 2 shows the influence of  $E1$ - $M2$  interference on the degree of linear polarization  $P$  as functions of the incident electron energy for the  $2p_{3/2} \rightarrow 1s_{1/2}$  transition line of H-like  $\text{Mo}^{41+}$ ,  $\text{Au}^{78+}$ , and  $\text{U}^{91+}$  ions and the  $2s_{1/2}2p_{3/2}(J=1) \rightarrow 1s_{1/2}2s_{1/2}(J=1)$  transition line of He-like  $\text{Mo}^{40+}$ ,  $\text{Au}^{77+}$ , and  $\text{U}^{90+}$  ions. For comparison, we also include in this figure the results without the  $E1$ - $M2$  interference effect. For the Lyman- $\alpha_1$  ( $2p_{3/2} \rightarrow 1s_{1/2}$ ) line of H-like ions, as shown in Figs. 2(a)–2(c), the linear polarization both with (labeled E1 + M2) and without (labeled E1) the interference effects decrease as the incident electron energy increases. The  $E1$ - $M2$  interference has a larger effect and makes the linear polarization decrease near the threshold, while these effects become less important with increasing incident electron energy. For example, for H-like  $\text{Mo}^{41+}$  ions, the interferential and noninterferential curves are very close to each other at all energies, but the interferential results are slightly below the noninterferential results. For the other H-like ions with higher atomic numbers, they have the same pattern but the near-threshold polarization decreases rapidly as the atomic number increases when interference effects are taken into account. The contribution of  $E1$ - $M2$  interference effects to linear polarization for the H-like  $\text{Mo}^{41+}$ ,  $\text{Au}^{78+}$ , and  $\text{U}^{91+}$  ions are 4%, 10%, and 16% at about 1.2 times the threshold energy and 2%, 7%, and 10% at 3 times the threshold energy, respectively.

For the  $2s_{1/2}2p_{3/2}(J=1) \rightarrow 1s_{1/2}2s_{1/2}(J=1)$  transition line of He-like ions, however, the linear polarization  $P$

increases with increasing incident electron energy. The  $E1$ - $M2$  interference effects make the linear polarization increase and become more and more important with increasing incident electron energy for high- $Z$  ions. The contribution of the  $E1$ - $M2$  interference effects to the linear polarization of the He-like  $\text{Au}^{77+}$  and  $\text{U}^{90+}$  ions is 2% and 1% at about 1.2 times the threshold energy and 25% and 35% at 3 times the threshold energy, respectively. But for the He-like  $\text{Mo}^{40+}$  ion, there are some differences. That is, the  $E1$ - $M2$  interference effects cause the linear polarization to decrease at an energy range below 2 times the threshold energy before starting to increase at higher incident electron energies. Polarizations with and without interference effects are 0 at 2.1 times the threshold energy. The contribution of the  $E1$ - $M2$  interference effects to the linear polarization of He-like  $\text{Mo}^{40+}$  is 6% at about 1.2 times the threshold energy and 5% at 3 times the threshold energy, respectively.

In Fig. 3, the polarizations with and without  $E1$ - $M2$  interference effects at 1.2 times the threshold energy for the H-like  $2p_{3/2} \rightarrow 1s_{1/2}$  transition line and at 3 times the threshold energy for the He-like  $2s_{1/2}2p_{3/2}(J=1) \rightarrow 1s_{1/2}2s_{1/2}(J=1)$  transition line are displayed versus the atomic number. In the figure, we can clearly see that the  $E1$ - $M2$  interference effects decrease the degree of linear polarization for H-like ions, while increasing it for He-like ions. Furthermore, we can see that the degree of linear polarization with only electric-dipole approximation changes relatively slowly with a low rate, while with  $E1$ - $M2$  interference effects the degree changes rapidly with increasing atomic number for both H-like and He-like ions. It appears, thus, that the differences between the degree of linear polarization with and that without  $E1$ - $M2$  interference effects at the given energies become more evident with increasing atomic number.



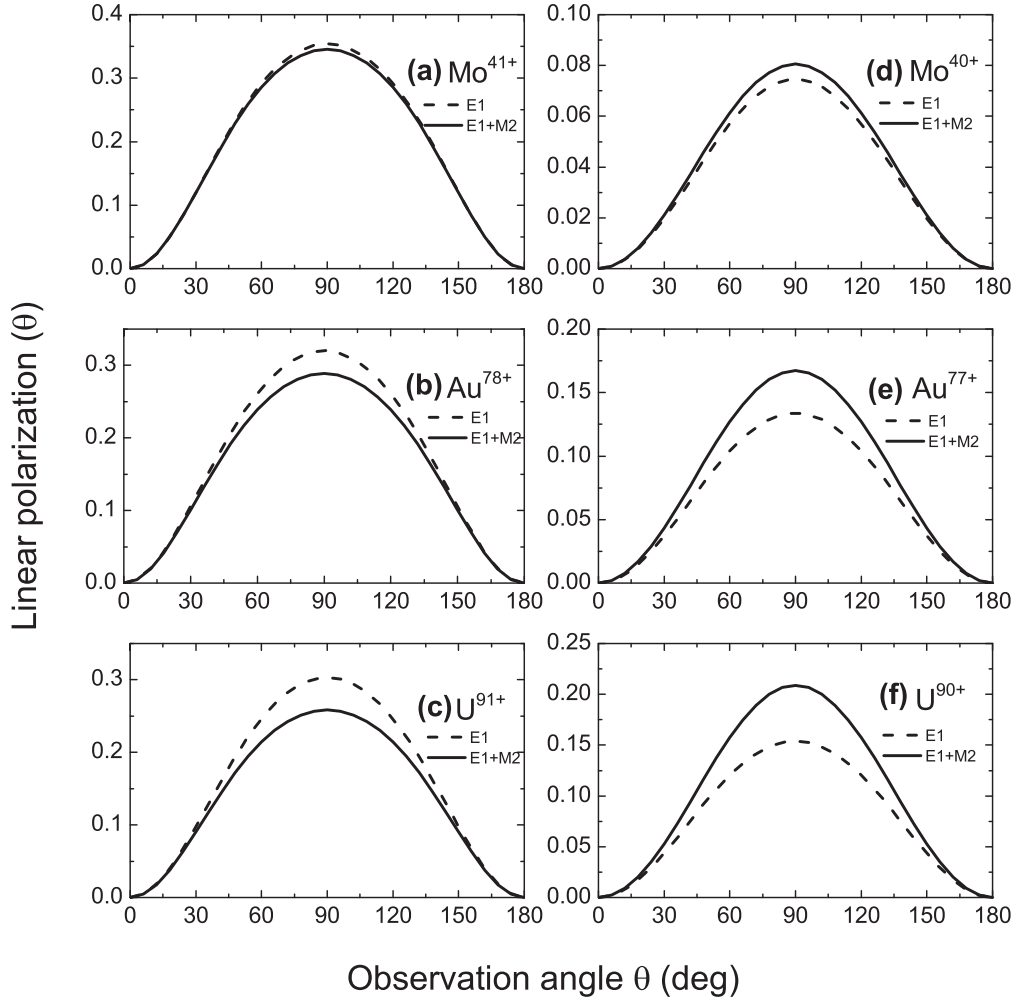


FIG. 4. The degree of linear polarization of the transition line  $2p_{3/2} \rightarrow 1s_{1/2}$  for H-like (left) and the transition line  $2s_{1/2}2p_{3/2}(J=1) \rightarrow 1s_{1/2}2s_{1/2}(J=1)$  for He-like (right) molybdenum, gold, and uranium ions as a function of the observation angle  $\theta$  relative to the electron beam. E1 + M2 represents values with inclusion of  $E1$ - $M2$  interference, and E1 represents inclusion of only the electric-dipole approximation.

#### D. The influence of interference on the angular distribution of linear polarization

In Fig. 4, we show the dependence of linear polarization on the angle  $\theta$  for the  $2p_{3/2} \rightarrow 1s_{1/2}$  transition line of H-like  $\text{Mo}^{41+}$ ,  $\text{Au}^{78+}$ , and  $\text{U}^{91+}$  ions at 1.2 times the threshold energy and the  $2s_{1/2}2p_{3/2}(J=1) \rightarrow 1s_{1/2}2s_{1/2}(J=1)$  transition line of He-like  $\text{Mo}^{40+}$ ,  $\text{Au}^{77+}$ , and  $\text{U}^{90+}$  ions at 3 times the threshold energy. As shown in Fig. 4, it is obvious that the maximum polarization occurs at  $\theta = 90^\circ$  in all cases and the differences between the results with and those without interference effects become increasingly pronounced as  $\theta$  tends to  $90^\circ$ . For the  $2p_{3/2} \rightarrow 1s_{1/2}$  line of H-like ions, the  $E1$ - $M2$  interference effects on the angular distribution of linear polarization become more and more important with increasing atomic number; especially, for  $\text{U}^{91+}$  ions, the effects can reduce the angular distribution of linear polarization by about 16% at  $\theta = 90^\circ$ . These characters are quite similar to the case of REC into initially bare uranium ions pointed out by Weber *et al.* [42]. In that case,  $E1$ - $M2$  multipole mixing reduces the degree of linear polarization by about 15% for observation angles near  $90^\circ$ , compared to the  $E1$ -only approach, and the result is in excellent agreement with their experimental data.

For the  $2s_{1/2}2p_{3/2}(J=1) \rightarrow 1s_{1/2}2s_{1/2}(J=1)$  transition line of He-like ions, as shown in Figs. 4(d)–4(f), interference effects make the angular distribution of linear polarization increase at the given incident electron energies. And this situation also becomes more and more important with increasing atomic number.

#### E. The influence of interference on the angular distribution of photoemission

To examine the influence of  $E1$ - $M2$  interference on the angular distribution of photoemission, we calculated the  $W(\theta)/\langle W \rangle$  ratio versus the angle  $\theta$  both with and without  $E1$ - $M2$  interference effects for the  $2p_{3/2} \rightarrow 1s_{1/2}$  transition line of H-like of  $\text{Mo}^{41+}$ ,  $\text{Au}^{78+}$ , and  $\text{U}^{91+}$  ions at 1.2 times the threshold energy and the  $2s_{1/2}2p_{3/2}(J=1) \rightarrow 1s_{1/2}2s_{1/2}(J=1)$  transition line of He-like  $\text{Mo}^{40+}$ ,  $\text{Au}^{77+}$ , and  $\text{U}^{90+}$  ions at 3 times threshold. The results are presented in Fig. 5. For the  $2p_{3/2} \rightarrow 1s_{1/2}$  line of H-like ions, as shown in Figs. 5(a)–5(c),  $E1$ - $M2$  interference effects can lead to a slight increase in the anisotropy of the intensity angular distribution, contrary to polarization. These characters mean that the dominant photon

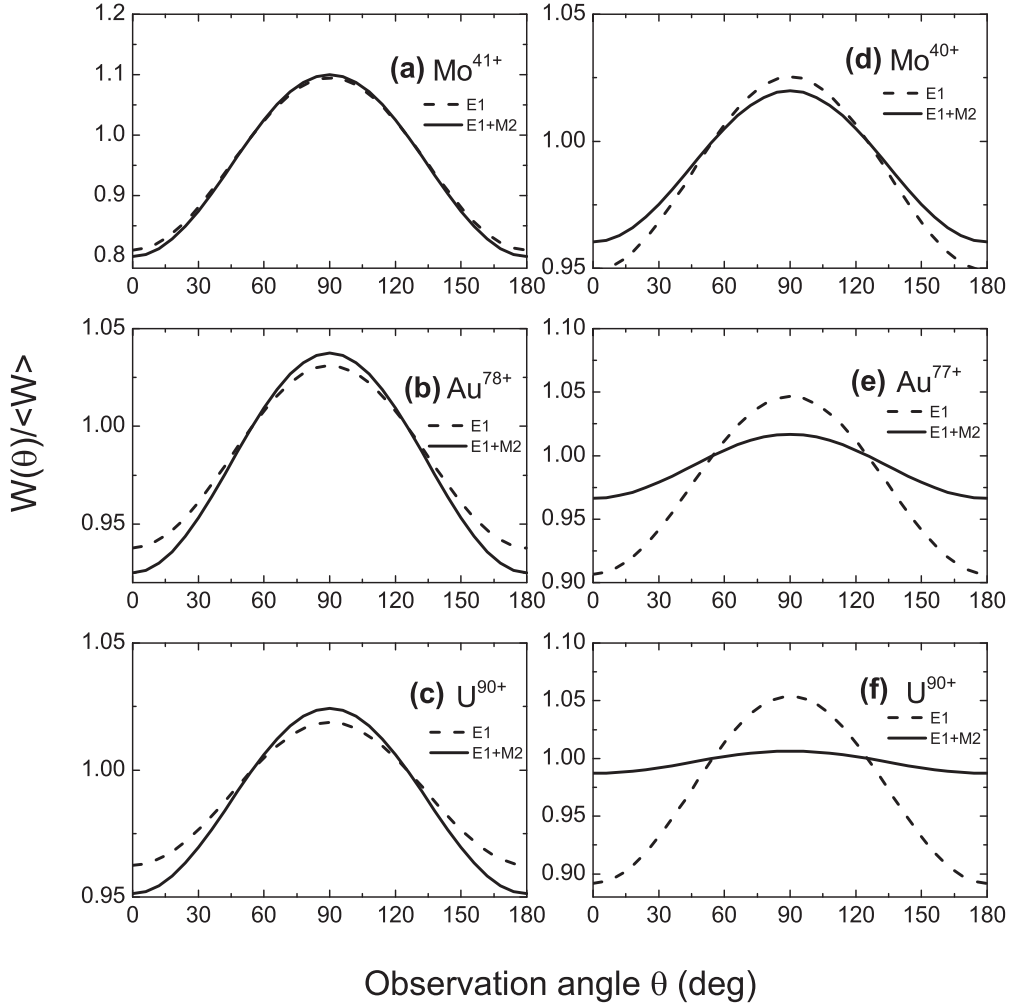


FIG. 5.  $W(\theta)/\langle W \rangle$  ratio for the transition line  $2p_{3/2} \rightarrow 1s_{1/2}$  of H-like (left) and the transition line  $2s_{1/2}2p_{3/2}(J=1) \rightarrow 1s_{1/2}2s_{1/2}(J=1)$  of He-like (right) molybdenum, gold, and uranium ions as a function of the observation angle  $\theta$  relative to the electron beam. E1 + M2 represents values with inclusion of  $E1$ - $M2$  interference, and E1 represents inclusion of only the electric-dipole approximation.

emission perpendicular to the electron beam including the  $E1$ - $M2$  interference has been enhanced. The contributions of the  $E1$ - $M2$  interference effects to the angular distribution of radiation  $W(\theta)/\langle W \rangle$  ratio at  $\theta = 90^\circ$  is 0.4%, 0.6%, and 0.9% for the H-like  $\text{Mo}^{41+}$ ,  $\text{Au}^{78+}$ , and  $\text{U}^{91+}$  ions, respectively. However, for He-like ions, as shown in Figs. 5(d)–5(f),  $E1$ - $M2$  interference effects lead to a reduction in the anisotropy of the angular distribution of radiation. And the dominant photon emission perpendicular to the electron beam, the inclusion of  $E1$ - $M2$  interference, clearly favors a collinear emission along the electron beam, contrary to H-like ions. The contributions of  $E1$ - $M2$  interference effects to the angular distribution of radiation at  $\theta = 90^\circ$  is about 1.2%, 3%, and 5% for the He-like  $\text{Mo}^{40+}$ ,  $\text{Au}^{77+}$ , and  $\text{U}^{90+}$  ions, respectively. Finally, we noted that the differences between the  $W(\theta)/\langle W \rangle$  ratio with and that without  $E1$ - $M2$  interference effects become more evident with increasing atomic number for both H-like and He-like ions.

In the above sections, we have studied the polarization properties and angular distribution of x-ray photoemission following direct impact excitation. Admittedly, besides the direct impact excitation, some other effects such as the resonance impact excitation may greatly affect the magnetic sublevel

cross sections and the linear polarizations of the corresponding lines for de-excitation processes in some cases [37]. However, according to our estimates, taking H-like  $\text{Mo}^{41+}$  ions, for example, in the present energy region, the resonance mainly comes from relatively high levels ( $nln'l', n, n' > 4$ ), whose corrections to the linear polarizations of the lines of interest are relatively small. These effects on the electron excitation and de-excitation processes are neglected in the present calculations, which could be a good approximation for the purposes of discussing the contributions of the magnetic quadrupole ( $M2$ ) to the subsequent characteristic x-ray emission.

#### IV. CONCLUSION

In summary, we have investigated the linear polarization and angular distribution of Lyman- $\alpha_1$  ( $2p_{3/2} \rightarrow 1s_{1/2}$ ) line of H-like  $\text{Mo}^{41+}$ ,  $\text{Au}^{78+}$ , and  $\text{U}^{91+}$  ions and  $2s_{1/2}2p_{3/2}(J=1) \rightarrow 1s_{1/2}2s_{1/2}(J=1)$  line of He-like  $\text{Mo}^{40+}$ ,  $\text{Au}^{77+}$ , and  $\text{U}^{90+}$  ions following EIE processes using a fully RDW method. Emphasis is placed on the effects of  $E1$ - $M2$  interference on the polarization properties and angular distribution of radiation for subsequent x-ray emission. Our results show that the interfer-

ence of the  $E1$  decay and the  $M2$  decay can either decrease or enhance the degree of line polarization for the emitted x-rays, and these dramatic influences will also lead to a remarkable variation of the subsequent angular emission pattern, whose characters strongly depend on the atomic number and incident electron energy. For the Lyman- $\alpha_1$  ( $2p_{3/2} \rightarrow 1s_{1/2}$ ) line of H-like  $\text{Mo}^{41+}$ ,  $\text{Au}^{78+}$ , and  $\text{U}^{91+}$  ions, the contributions of  $E1$ - $M2$  interference effects to the linear polarization are 4%, 10%, and 16% and the contributions to the  $\theta = 90^\circ$  angular photoemission pattern are 0.4%, 0.6%, and 0.9% at about 1.2 times the threshold energy, respectively. For He-like  $2s_{1/2}2p_{3/2}(J=1) \rightarrow 1s_{1/2}2s_{1/2}(J=1)$  line of  $\text{Mo}^{40+}$ ,  $\text{Au}^{77+}$ , and  $\text{U}^{90+}$  ions, the contributions of  $E1$ - $M2$  interference effects to the linear polarization are 1%, 25%, and 35% at about

3 times the threshold energy, respectively. A dominant photon emission perpendicular to the electron beam clearly favoring a collinear emission along the electron beam has been found. We hope that with the development of experimental technology, such strong effects will become feasible in experiments by measuring either the polarization or the angular distribution of radiation emitted in the process of EIE of atoms or ions.

## ACKNOWLEDGMENTS

This work was supported by the National Natural Science Foundation of China (Grants No. 11274254, No. 11147018, and No. U1332206).

- 
- [1] J. Dubau, M. K. Inal, and A. M. Urnov, *Phys. Scripta* **T65**, 179 (1996).
  - [2] E. Haug, *Sol. Phys.* **61**, 129 (1979).
  - [3] E. Haug, *Sol. Phys.* **71**, 77 (1981).
  - [4] A. S. Shlyaptseva, S. B. Hansen, V. L. Kantsyrev, B. S. Bauer, D. A. Fedin, N. Ouart, S. A. Kazantsev, A. G. Petrashen, and U. I. Safronova, *Rev. Sci. Instrum.* **72**, 1241 (2001).
  - [5] J. C. Kieffer, J. P. Matte, H. Pépin, M. Chaker, Y. Beaudoin, T. W. Johnston, C. Y. Chien, S. Coe, G. Mourou, and J. Dubau, *Phys. Rev. Lett.* **68**, 480 (1992).
  - [6] J. C. Kieffer, J. P. Matte, M. Chaker, Y. Beaudoin, C. Y. Chien, S. Coe, G. Mourou, J. Dubau, and M. K. Inal, *Phys. Rev. E* **48**, 4648 (1993).
  - [7] P. Hakel, R. C. Mancini, J.-C. Gauthier, E. Mínguez, J. Dubau, and M. Cornille, *Phys. Rev. E* **69**, 056405 (2004).
  - [8] Y. Inubushi, T. Kai, T. Nakamura, S. Fujioka, H. Nishimura, and K. Mima, *Phys. Rev. E* **75**, 026401 (2007).
  - [9] P. Hakel, R. C. Mancini, J. Abdallah, M. E. Sherrill, and H. L. Zhang, *J. Phys. B* **42**, 085701 (2009).
  - [10] J. R. Henderson, P. Beiersdorfer, C. L. Bennett, S. Chantrenne, D. A. Knapp, R. E. Marrs, M. B. Schneider, K. L. Wong, G. A. Doschek, J. F. Seely, C. M. Brown, R. E. LaVilla, J. Dubau, and M. A. Levine, *Phys. Rev. Lett.* **65**, 705 (1990).
  - [11] P. Beiersdorfer, D. A. Vogel, K. J. Reed, V. Decaux, J. H. Scofield, K. Widmann, G. Hölzer, E. Förster, O. Wehrhan, D. W. Savin, and L. Schweikhard, *Phys. Rev. A* **53**, 3974 (1996).
  - [12] E. Takács, E. S. Meyer, J. D. Gillaspy, J. R. Roberts, C. T. Chantler, L. T. Hudson, R. D. Deslattes, C. M. Brown, J. M. Laming, J. Dubau, and M. K. Inal, *Phys. Rev. A* **54**, 1342 (1996).
  - [13] A. S. Shlyaptseva, R. C. Mancini, P. Neill, and P. Beiersdorfer, *Rev. Sci. Instrum.* **68**, 1095 (1997).
  - [14] P. Beiersdorfer, J. C. López-Urrutia, V. Decaux, K. Widmann, and P. Neill, *Rev. Sci. Instrum.* **68**, 1073 (1997).
  - [15] P. Beiersdorfer, G. Brown, S. Utter, P. Neill, K. J. Reed, A. J. Smith, and R. S. Thoe, *Phys. Rev. A* **60**, 4156 (1999).
  - [16] F. Walden, H.-J. Kunze, A. Petoyan, A. Urnov, and J. Dubau, *Phys. Rev. E* **59**, 3562 (1999).
  - [17] N. Nakamura, D. Kato, N. Miura, T. Nakahara, and S. Ohtani, *Phys. Rev. A* **63**, 024501 (2001).
  - [18] D. L. Robbins, A. Ya. Faenov, T. A. Pikuz, H. Chen, P. Beiersdorfer, M. J. May, J. Dunn, K. J. Reed, and A. J. Smith, *Phys. Rev. A* **70**, 022715 (2004).
  - [19] D. L. Robbins, P. Beiersdorfer, A. Ya. Faenov, T. A. Pikuz, D. B. Thorn, H. Chen, K. J. Reed, A. J. Smith, K. R. Boyce, G. V. Brown, R. L. Kelley, C. A. Kilbourne, and F. S. Porter, *Phys. Rev. A* **74**, 022713 (2006).
  - [20] Y. M. Liu, S. Singha, T. E. Witt, Y. T. Cheng, and R. J. Gordon, *Appl. Phys. Lett.* **93**, 161502 (2008).
  - [21] K. J. Reed and M. H. Chen, *Phys. Rev. A* **48**, 3644 (1993).
  - [22] C. J. Fontes, H. L. Zhang, and D. H. Sampson, *Phys. Rev. A* **59**, 295 (1999).
  - [23] L. Sharma, A. Surzhykov, R. Srivastava, and S. Fritzsche, *Phys. Rev. A* **83**, 062701 (2011).
  - [24] P. Amaro, F. Fratini, S. Fritzsche, P. Indelicato, J. P. Santos, and A. Surzhykov, *Phys. Rev. A* **86**, 042509 (2012).
  - [25] Y. Itikawa, R. Srivastava, and K. Sakimoto, *Phys. Rev. A* **44**, 7195 (1991).
  - [26] M. K. Inal and J. Dubau, *J. Phys. B* **20**, 4221 (1987).
  - [27] M. K. Inal, H. L. Zhang, and D. H. Sampson, *Phys. Rev. A* **46**, 2449 (1992).
  - [28] M. K. Inal and J. Dubau, *Phys. Rev. A* **47**, 4794 (1993).
  - [29] M. K. Inal, D. H. Sampson, H. L. Zhang, and J. Dubau, *Phys. Scripta* **55**, 170 (1997).
  - [30] M. K. Inal, H. L. Zhang, D. H. Sampson, and C. J. Fontes, *Phys. Rev. A* **65**, 032727 (2002).
  - [31] M. K. Inal, A. Surzhykov, and S. Fritzsche, *Phys. Rev. A* **72**, 042720 (2005).
  - [32] T. Kai, R. Srivastava, and S. Nakazaki, *Phys. Rev. A* **70**, 062705 (2004).
  - [33] T. Kai, S. Nakazaki, and K. A. Berrington, *Nucl. Instrum. Methods Phys. Res. B* **235**, 249 (2005).
  - [34] T. Kai, S. Nakazaki, T. Kawamura, H. Nishimura, and K. Mima, *Phys. Rev. A* **75**, 012703 (2007).
  - [35] T. Kai, S. Nakazaki, T. Kawamura, H. Nishimura, and K. Mima, *Phys. Rev. A* **75**, 062710 (2007).
  - [36] Z. Q. Wu, Y. M. Li, B. Duan, J. Yan, and H. Zhang, *Chin. Phys. Lett.* **24**, 1560 (2007).
  - [37] J. Jiang, C. Z. Dong, L. Y. Xie, and J. G. Wang, *Phys. Rev. A* **78**, 022709 (2008).
  - [38] M. H. Chen and J. H. Scofield, *Phys. Rev. A* **52**, 2057 (1995).



- [39] S. Fritzsche, A. Surzhykov, and T. Stöhlker, *Phys. Rev. Lett.* **103**, 113001 (2009).
- [40] R. Bensaid, M. K. Inal, and J. Dubau, *J. Phys. B* **39**, 4131 (2006).
- [41] A. Surzhykov, S. Fritzsche, A. Gumberidze, and T. Stöhlker, *Phys. Rev. Lett.* **88**, 153001 (2002).
- [42] G. Weber, H. Bräuning, A. Surzhykov, C. Brandau, S. Fritzsche, S. Geyer, S. Hagmann, S. Hess, C. Kozhuharov, R. Martin, N. Petridis, R. Reuschl, U. Spillmann, S. Trotsenko, D. F. A. Winters, and T. Stöhlker, *Phys. Rev. Lett.* **105**, 243002 (2010).
- [43] A. Surzhykov, Y. Litvinov, T. Stöhlker, and S. Fritzsche, *Phys. Rev. A* **87**, 052507 (2013).
- [44] F. A. Parpia, C. F. Fischer, and I. P. Grant, *Comput. Phys. Commun.* **94**, 249 (1996).
- [45] J. Jiang, C. Z. Dong, L. Y. Xie, J. G. Wang, J. Yan, and S. Fritzsche, *Chin. Phys. Lett.* **24**, 691 (2007).
- [46] S. Fritzsche, H. Aksela, C. Z. Dong, S. Heinäsmäki, and J. E. Sienkiewicz, *Nucl. Instrum. Methods Phys. Res. B* **205**, 93 (2003).
- [47] H. L. Zhang, D. H. Sampson, and R. E. H. Clark, *Phys. Rev. A* **41**, 198 (1990).
- [48] H. L. Zhang and D. H. Sampson, *Phys. Rev. A* **66**, 042704 (2002).
- [49] V. G. Pal'chikov, *Phys. Scripta* **57**, 581 (1998).
- [50] [http://www.astronomy.ohio-state.edu/~nahar/nahar\\_radiativeatomicdata/index.html](http://www.astronomy.ohio-state.edu/~nahar/nahar_radiativeatomicdata/index.html).
- [51] S. N. Nahar, A. K. Pradhan, and S. Lim, *Can. J. Phys.* **89**, 483 (2011).
- [52] S. N. Nahar, A. K. Pradhan, and C. Sur, *J. Quant. Spectrosc. Radiat. Transf.* **109**, 1951 (2008).
- [53] C. J. Bostock, D. V. Fursa, and I. Bray, *Phys. Rev. A* **80**, 052708 (2009).